2.7 Insertion devices

2.7.1 Introduction

The Cornell ERL is designed for up to 14 x-ray beamlines with undulator magnets used as radiation sources. The type of the undulator magnet for each beamline is based on the beam line purpose. Tab. 2.7.1 lists x-ray beamlines according to function with the required photon energy range and space available for the various IDs.

The unique properties of the ERL x-ray beams are determined by a high-quality electron beam passing through its insertion devices comprising periodic arrays of magnets or wire coils that 'wiggle' the beam, and in the process, produce the optimal hard and soft coherent x-ray beams for experimentation at the ERL facility.

Third-generation synchrotron radiation facilities have brought ID technology to a high state of optimization for storage-ring use. These developments form a solid base of principles and practices that can be advanced even further for ERL applications. The advancements involve optimizations to cover various photon energy ranges, taking advantage of the very small ERL source size, divergence, polarization control of the emitted x-rays, and ease of tunability. The ERL machine gives ID designers new freedom in its magnetics due to the interesting new machine properties. Since the ERL is not a storage ring, no extra horizontal aperture is required for injection and thus the ID magnets may be close to the electron beam. Small bore devices with an inner diameter of 5 mm or smaller are now practical.

The electron beam energy is high enough at 5 GeV and the emittance and energy spread are small enough to make small-period IDs perform exceptionally well. Undulators with small gaps (and therefore small periods down to about twice the gap dimension) become feasible. More periods per ID unit length mean more flux and spectral brightness per unit length.

In addition, the lattice and layout of the ERL can accommodate long ID lengths compared to standard storage-ring ID straights. The ERL's very low energy spread of $\Delta E/E$ of 2×10^{-4} means that constructive interference can be maintained even in 1000-period long devices. This is important not only for maintaining a very high average x-ray flux on the x-ray beamline, but may permit monochromator-less beamlines, thus removing all the optical issues of associated coherence preservation through the optics.

A further feature is the practical use of the higher harmonics of the x-ray spectrum for high-photon energy experiments (up to 80–100 keV), a scheme that is well-developed by the current third generation storage-ring sources.

There are, of course, concerns and optimizations for any technology that breaks new territory. Some of the design concerns for ERL insertion devices (as well as for many existing IDs) are:

- Cost per meter of the segment IDs
- Predicted reliability over a 10 year period
- Overall complexity of mechanics and magnetics
- Radiation damage resistance of undulator technology
- rms phase errors (in degrees) from period to period down the length of the device

Table 2.7.1: The 14 ID beamlines at Cornell's ERL. The beamlines are optimized for x-ray use in the indicated energy ranges. The purposes of the beamlines are indicated and range from coherent diffraction to several kinds of nanoprobes.

beamline	application	mode	ID length	E (keV)	BL length
Coherent diffraction and XPCS	Microscopy and dynamics at nm	Hi-Coh	25 m	5-25	80 m
Nanoscope, Nanoprobe	TXM/STXM with high NA	Hi-Coh	5 m	5-25	75 m
Soft x-ray	Microscope for biomaterials, XMCD nanomagnetic imaging, ARPES	Hi-Coh	5 m	0.1 - 5	75 m
Nanoprobe	General, 1 nm beam	Hi-Coh	5 m	1-10	80 m
Protein Crystallography I	High throughput, microfocus	Hi-flux	5 m	5-25	40 m
Protein Crystallography II	Wide range tunability	Hi-flux	5 m	5-25	40 m
Inelastic x-ray Scattering	1 meV resolution	Hi-flux	25 m	5-25	80 m
Femtosecond timing	Charge density waves	Ultra-fast	25 m	2-25	80 m
Materials Science I	High pressure science	Hi-flux	5 m	5-100	75 m
Materials Science II	General material science	Hi-flux	5 m	5-25	45 m
Resonant Scattering	x-ray science	Hi-flux	5 m	5-25	80 m
SAX I, XPCS, grazing incidence	Mesoscopic science	Hi-flux	5 m	5-25	80 m
SAX II	Mesoscope science	Hi-flux	5 m	5-25	80 m
Diagnostics	Beamsize and position measurements	All modes	5 m	5-25	40 m

- Ability to correct phase errors when observed
- Metrology to determine field qualities and errors from Hall probe, scanning wires, etc.
- Metrology to verify what has been produced and if the magnetic field qualities change over years of use
- Amount of development needed for prototypes and production versions
- What is the practical limit to useful harmonic number?
- How quickly (in hours or days) does it take to remove the device after a damage incident and replace it with a spare?

- Vacuum qualities - Does it take a lot of conditioning to get it ready to work in the ERL?
- How quickly (in minutes or seconds) will it take to tune from circular to linear polarization?
- How reproducible will the magnetic fields be after a change from linear to circular polarization and back to linear again? (or for any other mechanical or temperature change)
- How can the trajectory be tuned so that the integral of B*dL over the device length is low enough not to disturb the ERL electron optics?
- How will beam image currents and HOMs be dealt with?
- Will separate quadrupoles and collimators be periodically needed along the 25 m ID magnetic length device? What are the magnetic field tolerances needed for a 1000-pole undulator to have a relative line width equal to 1 divided by the number of periods? What are the operating and maintenance costs predicted to be over the life of the ID?

The ERL insertion device group is investigating insertion devices based on pure permanent technology as well superconducting technology. The state of progress in each of these areas is discussed in the next two sections.

2.7.2 Permanent magnet insertion devices

General remarks

ERL insertion devices based on permanent magnets (PM) are being designed to take advantage of unique ERL operational characteristics. In contrast to storage rings, an ERL does not require additional space around electron beams for newly injected particles. Thus, the beam aperture size (and the ID gap) can be significantly reduced and made round. This feature alone allows placement of magnetic material very close to the beam axis as well as permitting a symmetrical magnetic structure around the electron beam. The consequence of a smaller gap is a stronger magnetic field. The opportunity for a magnetic structure with 4-fold symmetry simplifies construction and magnetic field tuning. Both of these features are incorporated into the Delta undulator design.

The Delta design may also be useful for Free Electron Laser (FEL) applications. Although ERL and FEL machines use the same type of electron beam and their operations are similar, the ID requirements are quite different for each application. Early FEL undulators were generally not adjustable in their magnetic field value and the x-ray energy was adjusted by varying the energy of electron beam. This is not practical with an ERL facility where it is important to provide x-rays with various energies for several experimental stations working simultaneously and to dynamically tune the photon energy as the experiment progresses. Another significant difference between FEL and ERL machines is that the average beam current in the Cornell ERL is planned to be two orders of magnitude larger than at an XFEL such as the LCLS and consequently the beam-generated heat load inside the ID is much higher.

Two candidates for permanent magnet ID designs that can be used at an ERL are considered. The prime candidate is of an innovative ‘Delta’ type. A second plan is to adapt a more conservative in-vacuum planar-type undulator approach.

State of the art

At present, the brightest x-ray beams are generated by planar undulators based on permanent magnet (PM) technology. Advanced types of PM undulators developed recently are listed below.

In-vacuum undulators (IVU)

The first in-vacuum undulator was constructed and put into operation at KEK (Japan) in 1991 [1]. IVUs have magnet arrays enclosed in a vacuum vessel. The enclosure eliminates the need for the vacuum beam pipe inside the ID and allows reduction of the undulator gap down to a size of a few millimeters. Smaller gaps allow for a stronger magnetic field, which in turn can be translated into a device with more poles per unit length and, as a consequence, can produce more x-ray flux and higher x-ray brightness than larger gap devices. Presently the IVU technology is well established. In-vacuum undulators are considered standard devices at ESRF [2], [3] and other laboratories. The IVU operating at NSLS beamline X25 has the smallest gap of 3.3 mm [4].

Cryogenic permanent magnet undulators

Cryogenic Permanent Magnet Undulators (CPMU) have evolved directly from the IVU type. In [5], the authors propose to utilize a $\sim 20\%$ increase in the remnant field strength of NdFeB PM material as well as significant increases in the intrinsic coercivity at cryogenic temperatures of $\sim$ 150 K. The latter characteristic is critical for the magnet to resist radiation damage coming from the nearby electron beam. A CPMU prototype was developed, constructed, [6] and installed in a storage ring at ESRF. First operational experiences and performance studies are described in [7]. The main operational concerns are the temperature gradients across the magnetic material arising from the beam-induced heat load and the impact of the undulator structure on the local beam vacuum. The temperature gradient across the magnet material causes a variation of the magnetic field strength, which may reduce the undulator performance. Vacuum degradation may result in production of bremsstrahlung radiation in the ID, which will be sent down the x-ray beamline. So far this undulator design has demonstrated reasonable performance.

General requirements for ERL IDs

Peak field and K-parameter requirement

The required x-ray energy range for the typical undulator in Tab. 2.7.1 extends from 5 to 25 keV with middle energy of around 15 keV. To provide reasonable photon flux in this range, the synchrotron radiation critical energy should be not less than 15 keV. Using an expression from reference [8], see p. 184:

$$\epsilon_c = 0.655\,\mathrm{keV}\,\left(\frac{E}{\mathrm{GeV}}\right)^2\left(\frac{B}{\mathrm{T}}\right) \tag{2.7.1}$$

and assuming a 5 GeV beam energy, one finds that the peak field should be 0.9 T or higher.

The maximum value of the undulator parameter K, ($K = 0.934 \cdot (B/\ \mathrm{T}) \cdot (\lambda/\,\mathrm{cm})$, where B is the peak field, and λ is the undulator period), can be derived from the requirement that the 1st and 3rd undulator radiation harmonics should overlap. The expression for photon energy in a planar undulator, see [8] p. 188, for the i^{th} harmonics is:

$$\epsilon_n = 9.49\,\mathrm{keV} \cdot i \cdot \left(\frac{E}{\mathrm{GeV}}\right)^2 \frac{1}{(1+\frac{1}{2}K^2)} \left(\frac{\lambda_\mathrm{p}}{\mathrm{mm}}\right)^{-1} \tag{2.7.2}$$

where λ_p is the undulator period length.

Knowing that at $K = 0.5$ the 1st harmonic photon flux will drop by 50% (see Table 1 in [8] p. 190) one can find that, to satisfy the 1st and 3rd harmonics overlap condition, the undulator parameter K should equal 2.25.

Optical phase errors (phase shaking)

According to [9], reduction of the photon flux of i^{th} undulator harmonics due to undulator phase errors can be estimated as:

$$\frac{dF_n}{F_n} \approx -i^2\,\theta^2 \tag{2.7.3}$$

where $\frac{dF_n}{F_n}$ is the normalized flux reduction and θ is the rms phase error. For a reduction $\frac{dF_n}{F_n} \sim 10\%$ and $i = 5$ (the maximum harmonic number planned for use), an rms phase error of 3.70° or less is required.

Orbit walk-off

Using the criterion that the orbit walk-off should not exceed 10% of the beam size inside the undulator, the walk-off error should be less than 1 μm. The actual tolerable walk-off error for each undulator will vary with the emittace produced by the specific operating mode and the chosen beta function.

PM radiation damage and ID life-time estimation

The radiation damage dose rate to the ID can be estimated assuming that the major source of radiation damage is only due to high energy electrons scattered from the residual gas inside of the ID. Starting from the small-angle Coulomb scattering cross-section

$$\frac{d\sigma}{d\Omega} = \frac{4\,Z^2}{\gamma^2}\,r_e^2 \frac{1}{(\theta^2+\theta_{\mathrm{min}}^2)^2} \tag{2.7.4}$$

where Z is the atomic number, γ the relativistic factor, and r_e the classical electron radius, the flux rate of high energy electrons through a cylindrical surface of radius a per unit length as a function of residual gas density n_{gas} , beam current I_e and distance s from the undulator upstream end:

$$F(s) = \frac{I_e}{e}\,n_{\mathrm{gas}}\,\frac{4\,Z^2}{\gamma^2}\,r_e^2\,\frac{s^2}{a^2} \tag{2.7.5}$$

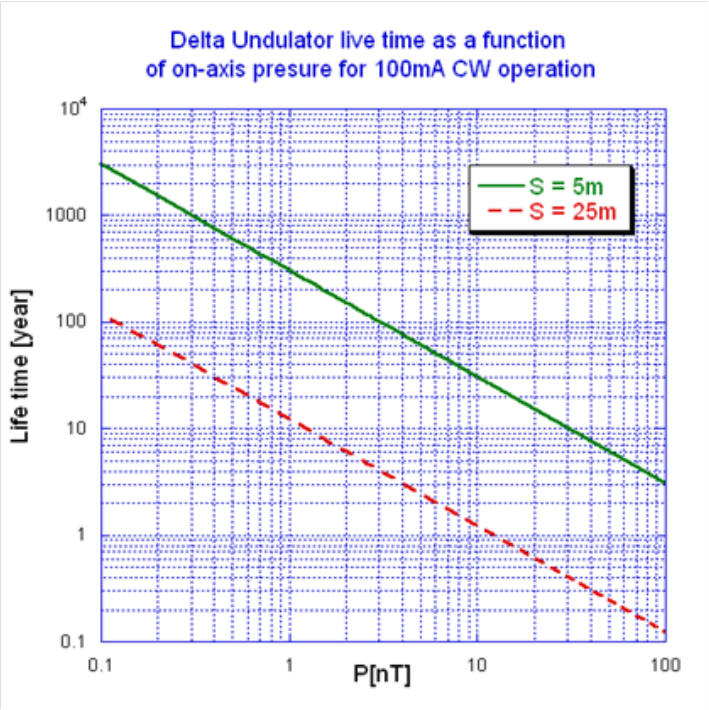

Figure 2.7.1: Estimated ID lifetime as function of on-axis pressure.

Assuming that residual gas content is similar to air, i.e. Z=7.5 (This is the worst possible scenario. In practice, in the absence of vacuum leaks, the content of residual gas is dominated by hydrogen with Z=1), 5 mm bore, 5 GeV beam energy and that all scattered electrons deposit energy into $\sim$ 5 mm layer around bore, the estimated rate of the dose accumulation is:

$$\dot{D}\left(\frac{\text{rad}}{\text{s}}\right) = 8.2 \times 10^{-5} \cdot \left(\frac{I_e}{\text{A}}\right) \cdot \left(\frac{P}{\text{nT}}\right) \cdot \left(\frac{s}{\text{m}}\right)^2 \tag{2.7.6}$$

Following [10], the estimated dose causing a 1% PM demagnetization at the downstream end of the PM undulators is 2 Mrad. Using this dose as a criterion, the dependence of the ID lifetime on the on-axis vacuum is shown in Fig. 2.7.1 It should be noted that although this estimate is made for a round bore ID like the Delta undulator, it can be applied to IDs with flat poles after small corrections.

Other general remarks

The undulator gap size is planned to be 5 mm. The choice is driven by the following arguments. The smaller gap results in a stronger magnetic field, which can be translated to a device with a shorter period, many more poles, and consequently a higher photon flux. However, the small gap will limit the access for magnetic field measurement, increase beam heat load and increase the risk of radiation damage due to beam losses. A 5 mm gap seems to be a reasonable compromise. The undulator period is dictated by the requirement of fundamental and third undulator harmonics overlap. For a 5 GeV beam energy, a 5 mm gap and NdFeB 40SH

magnetic material to provide harmonic overlap for $K = 2.25$, the undulator period should be $\sim$ 19 mm for a Delta and $\sim$ 24 mm for a PPM structure.

The choice of undulator length depends on many factors, including parameters of the magnetic measurement facility, and transportation capability. Shorter sections will be easier to build, tune, and transport. However, with longer sections available, the ID space can be used more efficiently. Both 2.5 m and 5 m lengths are under consideration at the present time. An in-vacuum configuration is a natural choice for 5 mm gap IDs. This type of undulator is well established. Operation at low temperature is preferable but not critical. As mentioned in the 'state of the art' section, ID operation at $\sim$ 120 K would increase PM intrinsic coercivity (H_{ci}) and increase the remnant field (B_r) by $\sim$ 10%. The first factor increases the resistance to radiation-induced demagnetization; the second would result in higher peak undulator field. In addition, lowering the magnet temperature would significantly reduce its out-gassing rate. This type of operation is presently under evaluation.

2.7.3 'Delta' undulator

The delta undulator was designed in anticipation of a new era of synchrotron radiation sources based on energy recovery Linac techniques [11]). The device is called a 'delta' undulator based upon the shape of its PM blocks, and makes optimum use of the unique conditions expected in the ERL. In comparison with conventional undulator magnets, it has:

- Full x-ray polarization control. It may generate various states of linearly polarized x-rays as well as left and right circular polarized x-rays with photon flux much higher than existing Apple–II type devices
- The delta design has 40% stronger magnetic field in linear and approximately two times stronger fields in circular polarization modes. These advantages translate into higher x-ray flux
- The undulator is very compact. The tested prototype was enclosed in a 25.4 cm diameter cylindrical vacuum vessel.

These advantages were achieved through a number of unconventional approaches. Among them is control of the magnetic field strength via longitudinal motion of the magnet arrays. The moving mechanism is also used for x-ray polarization control. The compactness is achieved using a recently developed permanent magnet soldering technique for fastening PM blocks.

Concept

Four identical magnet arrays assembled on base plates are symmetrically placed around the beam axis as illustrated on Fig. 2.7.2. One pair of magnet arrays generates vertical magnetic fields; another set of magnets generates the horizontal fields. Field strength is controlled by an adjustable phase (AP) scheme [12] where the peak field is controlled by moving the magnetic arrays relative to each other in the longitudinal (electron beam) direction. The same motion is used to control the polarization. To provide longitudinal displacement for the field strength and polarization control, magnet arrays are mounted on miniature rails attached to the thick plates, forming a rigid frame. In the linear polarization mode, the array pairs generating

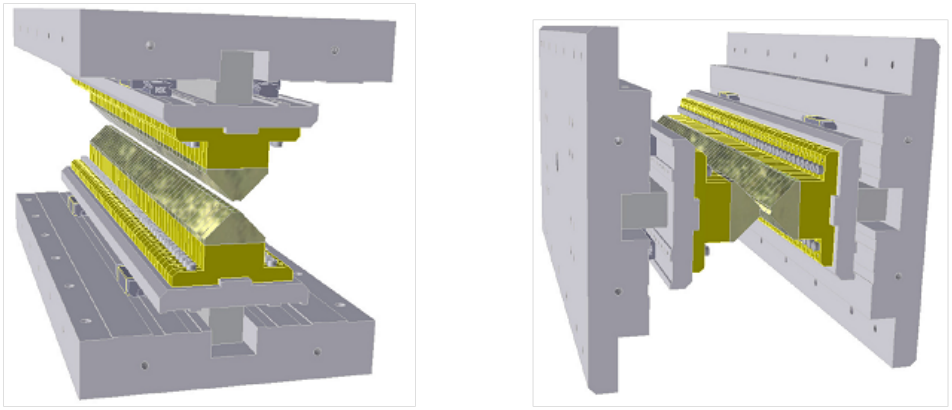

Figure 2.7.2: Two pairs of magnet arrays forming a Delta undulator structure. The left side shows arrays that generate the vertical field and the right side the horizontal.

vertical and horizontal magnetic fields are in phase. The resulting fields are planar and $\sqrt{2}$ stronger than those from a single pair. In the helical mode, the pairs are shifted relative to each other by 1/4 of a period or by 90^o, so the resulting field is helical. To change the field strength, two arrays forming the pair should be shifted longitudinally in opposite directions.

This arrangement can be considered as a combination of two independent AP undulators. It can also be viewed as a kind of Apple–III structure as mentioned in [13]. The Delta structure has similarities with the undulators described in[14] and [15] as well.

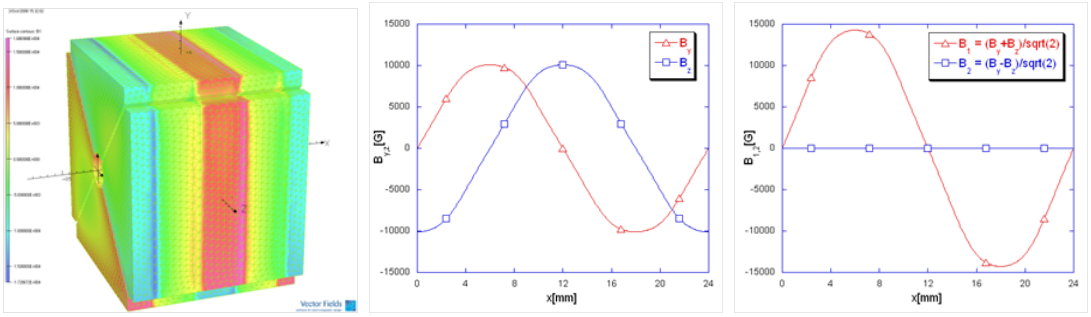

Figure 2.7.3: 3D model used in magnetic field modeling (left) and magnetic field components on beam axis for helical mode (middle) and planar mode (right) for 24 mm period.

Magnetic field properties

An example of 3D magnetic modeling is shown in Fig. 2.7.3 (left plot). The model has 5 mm diameter bore, 0.5 mm wide slits between magnetic arrays, and a NdFeB 40SH PM material with $B_r = 1.26$ T. The two other plots show magnetic field components along the beam axis for the helical and planer modes calculated for a 24 mm period. The peak field is 1.05 T in the helical mode (middle plot), when the horizontal field phase is shifted by 1/4 of a period

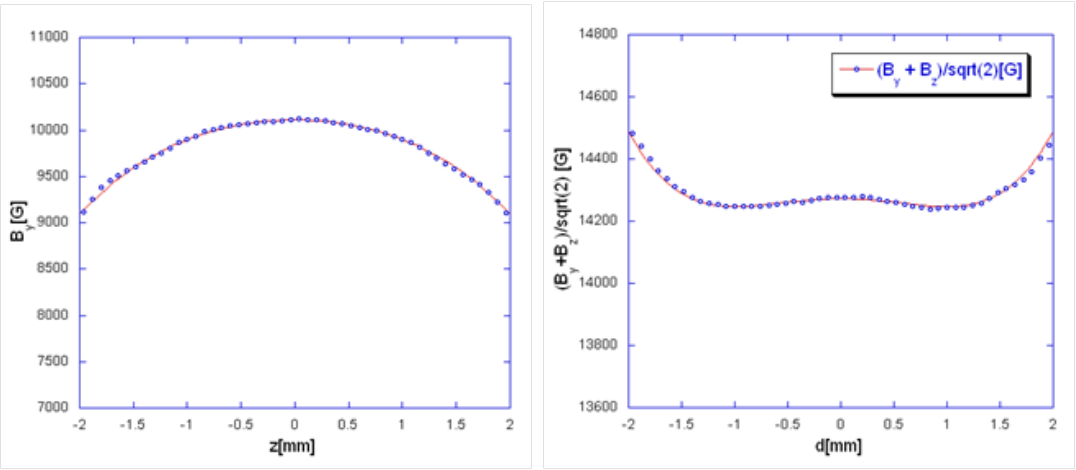

Figure 2.7.4: Field roll-off in helical (left) and planar (right) modes.

(90^o) relative to the vertical set of magnets. The calculated peak field is 1.43 T in the planar mode when both vertical and horizontal fields add in phase.

The field variation across the bore (roll-off) is calculated in Fig. 2.7.4. In the helical mode (left plot), the variation of the ±1 mm region around the central axis can be approximated by $dB/B \approx -0.02\, d^2/\,\mathrm{mm}^2$ where d is the distance from the axis. In planar mode, the field roll-off can be approximated as $dB/B \approx -0.0037\, d^2/\,\mathrm{mm}^2$. These variational formulas predict that 100 μm of misalignment of the undulator magnets relative to the beam axis (or beam trajectory relative undulator axis) will cause a $\sim\ 2 \times 10^{-4}$ variation of undulator K parameter in helical mode and 0.3×10^{-4} in planar mode. Both these variations due to magnet misalignments are acceptable.

Dependence of the peak field and undulator K parameter on the period for a 5 mm bore is depicted in Fig. 2.7.5 (left). The data indicate that fundamental and third-order undulator harmonics will be overlapping at a 19 mm period ($K = 2.25$ criteria). The plot on the right side of Fig. 2.7.5 compares a Delta undulator peak field as a function of a gap to period ratio with other PPM undulator magnet designs. The data for comparison were taken from [16]. The advantage of the Delta structure is evident in the considerably higher peak fields in both the planar and helical modes.

Mechanical design and beam heating load

Mechanical properties of the Delta undulator structure were analyzed in [11] and tested in [17]. It was found that the undulator components experience the highest stress in the planar mode. The left plot in Fig. 2.7.6 depicts results of an ANSYS stress analysis made for the tested prototype model of an undulator frame operated in a planar mode. The illustration on the right side of Fig. 2.7.6 shows the simulated effect of a heat load generated by the beam image current [11]. The temperature rise of the top of the magnets should not exceed 0.20°C at a maximum of 28 W/m of ERL beam-induced heat–loading relative cooling elements attached to the underside of the magnet arrays.

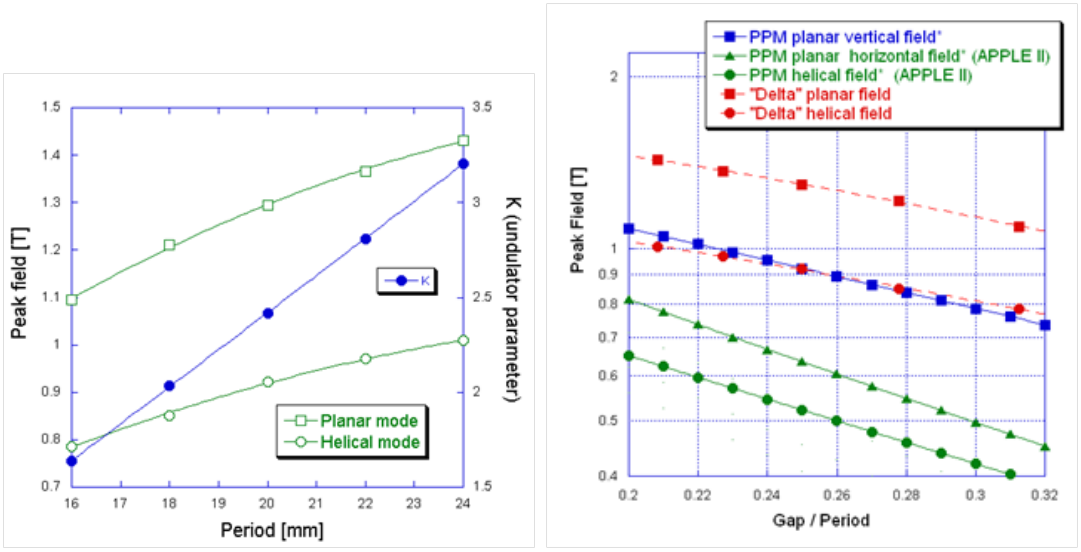

Figure 2.7.5: Left plot – peak field in planar and helical modes and undulator parameter K as a function of period. Right plot – peak field as function of gap over period ratio for 'Delta' and others PPM undulators.

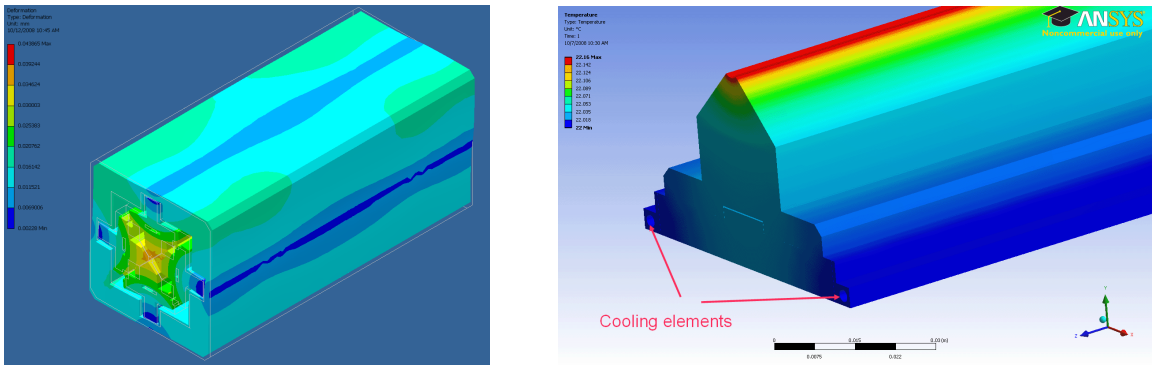

(a) Frame deformation

(b) Heat load

Figure 2.7.6: (a) Undulator frame deformation in the planar mode ranging from 3 μm to 44 μm, and (b) results of heat load analysis holding the device at 22°C with a maximum increase of 0.16°C.

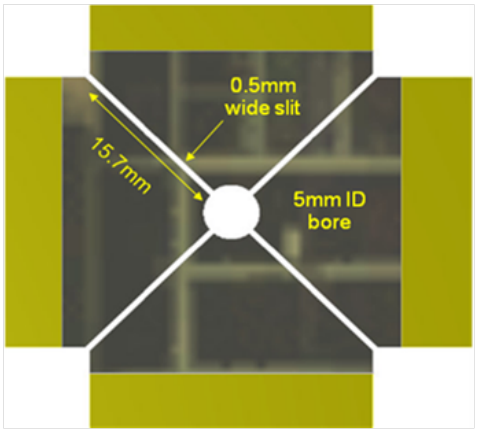

Figure 2.7.7: Delta undulator structure cross-section with ventilation channels dimensions.

On-axis vacuum considerations

The on-axis vacuum can be estimated in the following way. Fig. 2.7.7 depicts the Delta undulator cross section with its important dimensions.

The on-axis region is connected to the well-pumped outer volume by four channels of 0.5 mm width and 15.7 mm long length. A total molecular conductance (C) for four channels can be determined by using data in [18]. For the given geometry, the data imply $C \sim 0.278$ L/s per cm of structure length. The Ni–plated, PM-blocks out-gassing rate has been studied in [19]. An out-gassing rate (R) of less than 4×10^{-12} Torr/L/sec/cm^2 was observed after 48 hours of 120 C baking. The pressure differential between the central on-axis region and outside can be estimated as:

$$dP = \frac{AR}{C} = \frac{3.1415 \cdot 0.05 \cdot (4 \times 10^{-12})}{0.278} = 2.26 \times 10^{-11} \text{ Torr} = 0.022 \text{ nTorr} \qquad (2.7.7)$$

This pressure difference is acceptable.

Prototyping results

To verify basic principles of the design, a 30 cm long prototype model was built and tested. The two pictures on Fig. 2.7.8 illustrate the model. The left picture shows the undulator cross section with the Delta shape PM blocks forming a round bore installed in a box–like frame. The picture to the right shows three of four magnet arrays installed during assembly.

Magnetic field properties

Each magnet array was tuned individually to have optical phase errors of 3 degrees rms or less prior to final assembly. After the assembly was complete, the magnetic field was measured with the special setup described in [17]. Fig. 2.7.9 and Fig. 2.7.10 show the field components, the resultant calculated beam trajectory, and the on-axis X–ray spectra calculated for the field. Figure 2.7.9 presents this data for both helical modes. Figure 2.7.10 shows this information for a planar mode. Both helical model modes demonstrated a 0.91 T peak field (90% of the

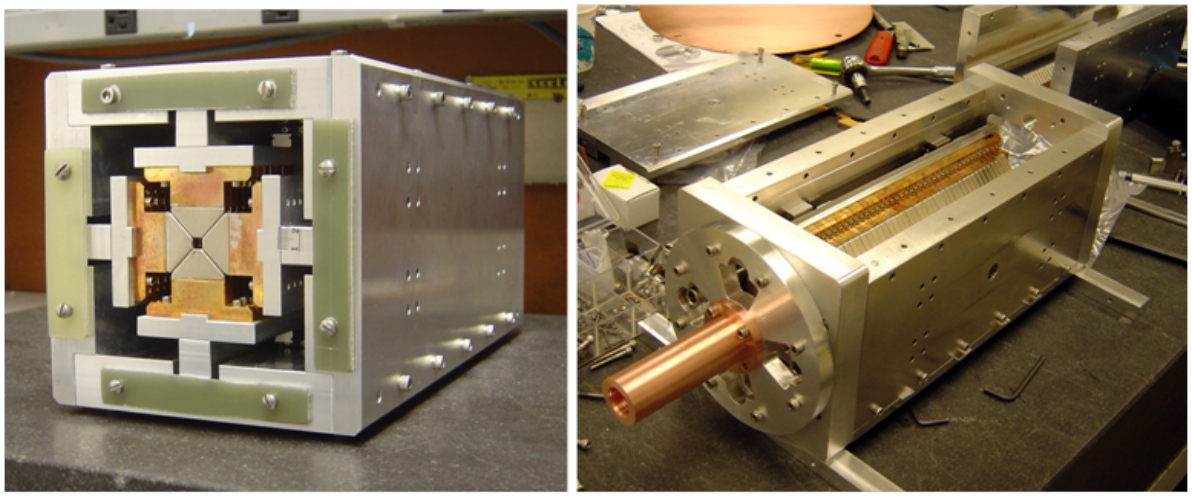

Figure 2.7.8: Delta undulator model in assembly process.

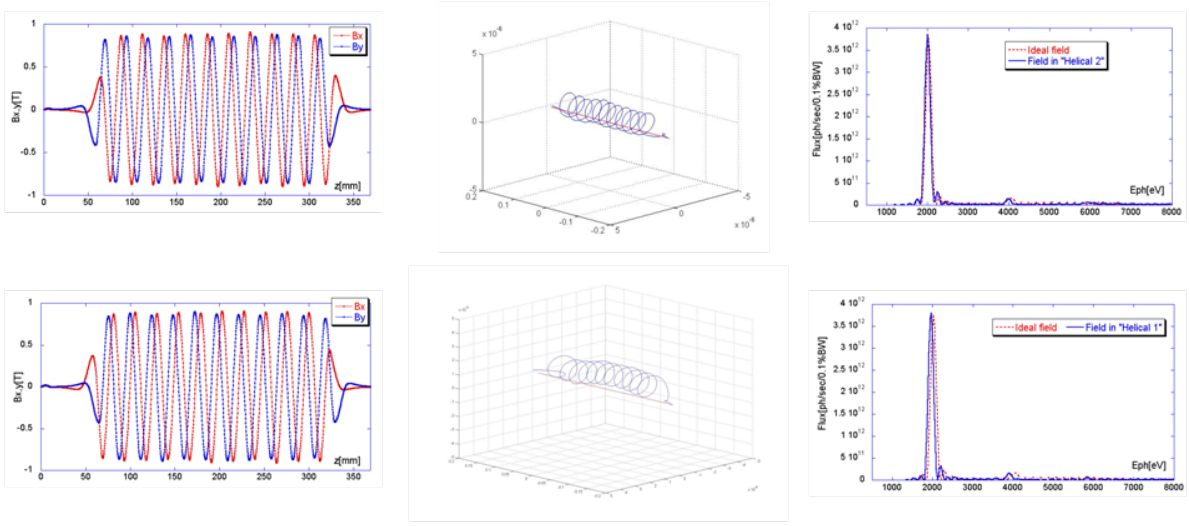

Figure 2.7.9: Left plots show vertical and horizontal field components measured in both helical modes corresponding to left and right x-ray polarizations. Central plots are 3D trajectories calculated for 5 GeV beam using measured magnetic field. Right plots are on-axis x-ray photon spectra calculated for measured and ideal fields.

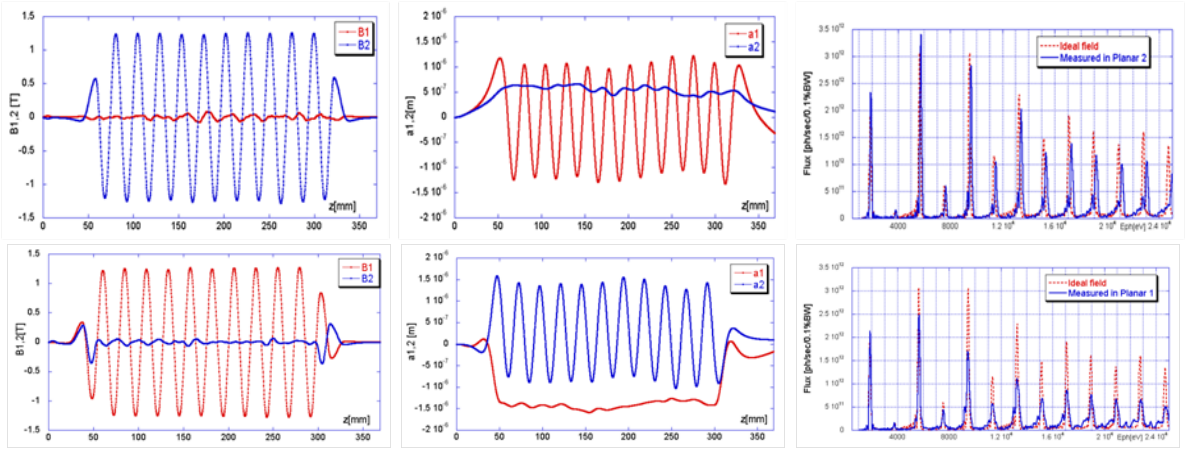

Figure 2.7.10: Measured magnetic field components (left), and predicted trajectories (center), and on-axis x-ray spectrum (right) in planar modes.

design). The negligible difference between x-ray spectra calculated for the measured and ideal fields indicated good field quality at this stage of development.

A peak field of 1.28 T was measured in a planar mode (89% of the design). The difference in spectra calculated for ideal and measured field (10% and 40% at 5^{th} harmonics) is probably due to a small shift of the magnet arrays in the transfer direction caused by a strong attractive magnetic force between adjoining arrays. This problem will be addressed and fixed in the next version of the device.

Vacuum properties

The magnet arrays were attached to the frame plates, enclosed in a vacuum vessel and pumped down in order to evaluate vacuum properties. The measured pressure was 4 nTorr after 100 hrs baking at 90 C with the very modest pumping speed of an 8 liters/sec. RGA spectral analysis indicated that 90% of the residual gas was H_2. Magnetic field measurement after the baking indicated no noticeable change in the magnetic field.

Beam test at the Accelerator Test Facility in BNL

The model undulator was tested with beam at the Accelerator Test Facility in Brookhaven National Laboratory at the end of 2009 ([20]). See Fig. 2.7.11.

Optical radiation was generated and observed on the fundamental undulator frequency from the device working in both helical and planar modes. The experimental results are compared with predictions in Fig. 2.7.12.

Data marked with circles on the left plot in Fig. 2.7.12 shows the measured dependence of the radiation intensity at a 5300 nm wavelength with electron beam energy and the Delta undulator in a planar mode. The dashed line represents the model calculation under an assumption of a 1.28 T peak undulator field. The sharp rise in intensity at a 55 MeV beam energy (due to the fundamental mode) is in agreement with observation.

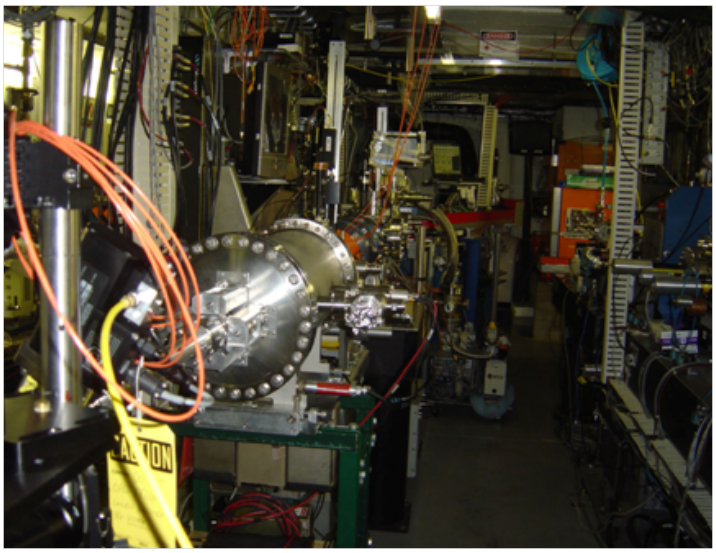

Figure 2.7.11: Delta undulator model installed in ATF beam line #2.

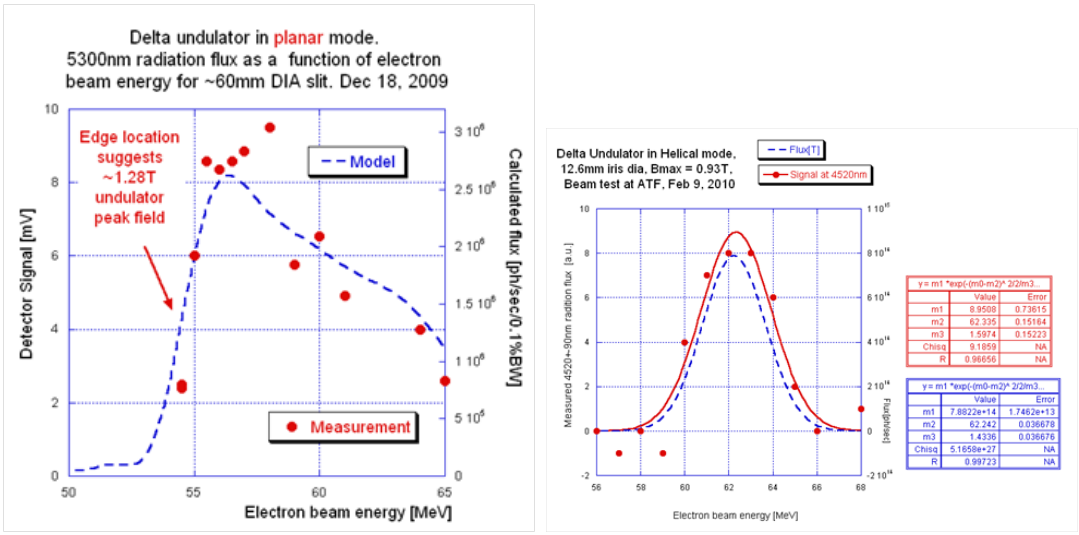

Figure 2.7.12: Radiation intensity measured at 5300 nm as a function of electron beam energy (left plot) with the Delta undulator in the planar mode. Radiation intensity at 4500 nm wavelength (right plot) as a function of electron beam energy for the Delta undulator model in the helical mode.

The plot on the right side of Fig. 2.7.12 depicts experimental data and the model prediction for the Delta undulator operating in a helical mode producing 4520 nm radiation. The observed peak location of 62.3 MeV was calculated to be caused by a 0.93 T undulator peak field. This peak field value was measured with a Hall probe after the beam test was concluded and was in good agreement with the 0.93 T calculated value.

Planar undulator

Planar undulators are considered as a back-up plan for the Delta design. They have been in use in storage-ring and FEL facilities for a long time, are well understood, and using these is a conservative approach.

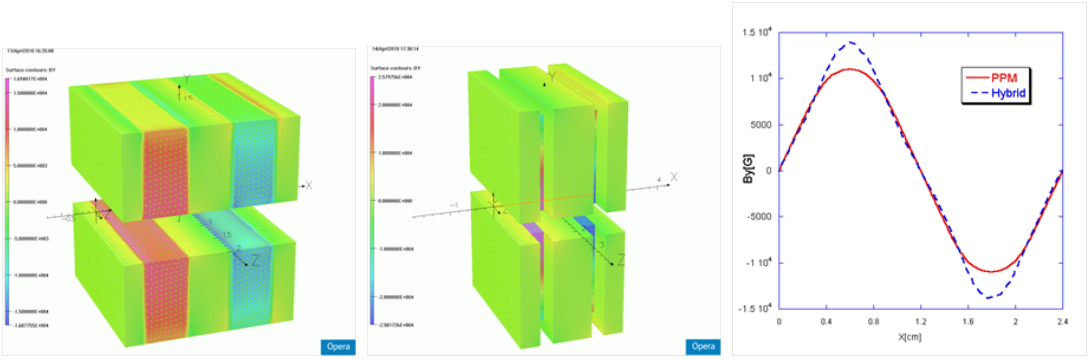

Figure 2.7.13: 3D models and field profile: PPM (left), Hybrid (center), magnetic field (right)

Magnetic structure modeling

Pure permanent magnet (PPM) structures were analyzed for the magnetic field formed by rectangular PM blocks magnetized in different directions. Hybrid structures can be made where magnetic blocks are combined with vanadium permendur poles. See Fig. 2.7.13. The left plot shows a PPM-type structure; the center plot is for a hybrid-type structure. All modeling results were obtained from the magnetic calculation code Opera–3D.

For equal gaps and periods, the hybrid structure demonstrated an approximately 20% higher magnetic field than a PPM structure. Although the hybrid structure has better field performance, its overall advantage is not obvious. It also has a stronger demagnetizing field, which elevates the risk of radiation damage and may limit the maximum temperature used during vacuum baking. The hybrid structure shows saturation effects in its poles, thus increasing its difficulties during operation and tuning. In addition, it requires more PM material and creates more mechanical stress.

Supporting structures

The AP scheme ([12]) can be used for the PPM case. Magnet arrays can be mounted inside a solid frame as depicted in Fig. 2.7.14 (left) on miniature rails that provide longitudinal motion. Mechanical drivers will be placed outside the vessel and mechanically coupled to the magnetic

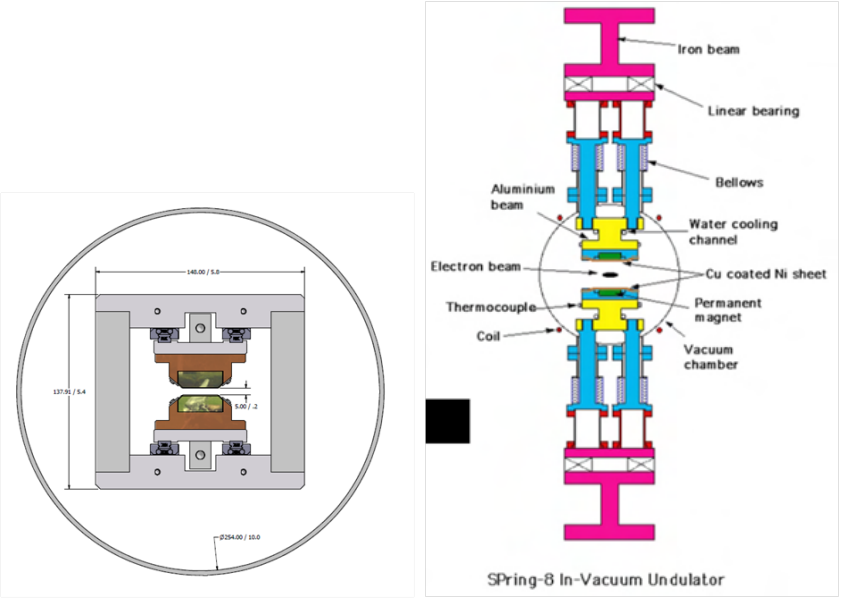

Figure 2.7.14: Supporting structures for PPM (left plot) and hybrid in–vacuum undulators (right). Vacuum chambers in both cases have similar dimensions.

arrays. Drivers should move arrays by at least 6 mm (1/4 undulator period) in both directions or more. The stress due to magnetic forces will be applied to the frame and driver components but not to the vacuum vessel. The initial analysis indicates the feasibility of such a scheme.

In the case of the hybrid-type magnetic structure, the magnetic field is controlled by a gap adjustment, a situation, Figure 2.7.14 (right), that requires a very large C–shaped supporting frame similar to the ones used at ESRF, SPring–8, and other laboratories. Thus the hybrid scheme is more expensive and takes up more space in comparison with the AP scheme. Taking all factors into account, the conclusion is that the PPM structure with the AP field control is preferable.

30-cm long Delta-undulator prototype summary and next steps

The novel Delta undulator technology is now in an advanced stage of prototyping. A 30 cm long in–vacuum prototype has successfully passed through early design stages including a first Linac beam test at the Accelerator Test Facility (ATF) facility at BNL.

The next step is to complete the engineering and fabrication work needed to scale the Delta design to a longer segment length. Segment lengths of 2.5 to 5 m are under consideration at the present time. The next round of development must also show how ERL beam image currents and HOMs will be satisfactorily dealt with on the curved inner surfaces next to the electron beam and how needed mechanical tolerances of the magnetic arrays can be held over distances greater than a meter in length.

2.7.4 Superconducting undulators

Undulators based on superconducting technology provide an alternative to PM technology for making insertion devices for the ERL. Insertion devices with superconducting (SC) windings of short period and small gap are known for producing some of the highest magnetic fields and thus could offer an opportunity for reaching the highest photon fluxes at energies of 100 keV or more. This is why these devices are under investigation by the ERL ID group.

Insertion devices with superconducting (SC) windings are well behaved under radiation exposure, as seen from their operation at the TEVATRON, LHC, CESR-B and Vepp2 damping ring [21]. We have considerable design, construction, and operational experience with SC wigglers installed at CESR [22, 23] and with undulators fabricated and tested at Cornell, [24] including a 4 m long device fabricated for an ILC positron source [25].

More recently, a SC workshop on undulators was held at Argonne National Laboratory, September 20–21, 2010 as a satellite workshop to SRI2010. Novel concept and fabrication ideas for SC undulators and wigglers were presented there for hard x-ray production [26]. Table 2.7.2 indicates the potential for an SC ID designed to produce higher field then a permanent magnet Delta ID, for the same gap and period. The change from helical to planar mode is accomplished by changing the current in the windings.

For the SC ID, rms phase error depends on accuracy in positioning SC wires. We estimate that a precision of 0.2 mm is feasible, leading to phase errors of less than 3°. The SC undulator uses two windings, of opposite helicity, to generate elliptical, circular and linearly polarized x-rays; a third winding of the same period but shifted by a half period can change the orientation of linear polarization. A K factor from 0 to 1.5 is possible with no mechanical motion for undulator periods of 15 to 25 mm and apertures of 5 to 8 mm. The early concept [27] has been applied to recent 3D magnetic designs using the MERMAID code [28]. Figure 2.7.15 shows a prototype SC double winding configuration undulator with the current directions indicated.

As was noted at the SC undulator workshop at Argonne, SC undulator research and development is being actively pursued at several locations around the world and advances can be expected; indeed, more research and development will be required for SC IDs to realize their ultimate promise.

For the purposes of this design study, it is sufficient to note that the permanent magnet undulators described in this document are already in an advanced state of development and are already on a path to achieve the x-ray beam characteristics specified for the ERL applications.

Table 2.7.2: Comparison between Delta and SC undulators. 5 mm clear bore diameter.

	$B_{\max}$ (T) in helical mode		$B_{\max}$ (T) in planar mode	
Period (mm)	Delta	SC	Delta	SC
24	1.0117	1.097	1.431	2.194
22	0.9686	1.058	1.37	2.194
20	0.9162	1.009	1.296	2.018
18	0.8533	0.9497	1.207	1.899
16	0.7787	0.8679	1.101	1.736

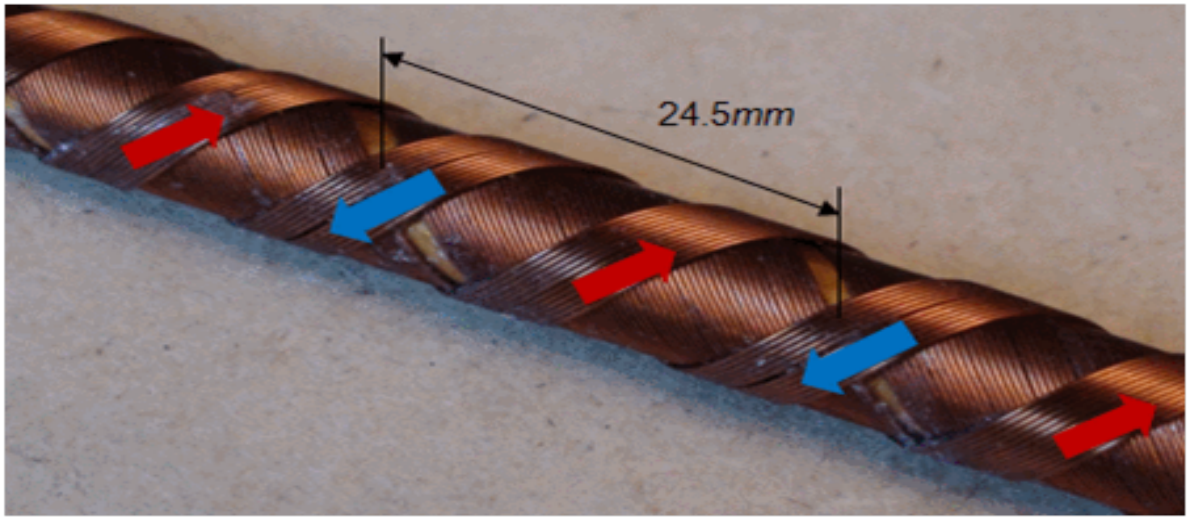

Figure 2.7.15: Coils wound over copper tube with six wire strands together in flat SC cable [26]. Period 24.5 mm. Outer diameter is 10 mm, inner diameter clear for beam is 8 mm. Direction of current in corresponding coil is shown by arrow

Obviously, if SC IDs develop to the point of practical utilization by the time of construction of an ERL facility, then they will be considered in the context of available undulators at that time. For now, the ERL ID group is continuing research and development on permanent magnet undulators specific to ERLs. SC undulator technology is making rapid progress, and could be included in the baseline design when construction of the ERL begins.

References

[1] Yamamoto, S., *et al. Construction of an in-vacuum type undulator for production of undulator x rays in the 5–25 keV region.* Review of Scientific Instruments, **63** (1), pages 400–403 (1992).

[2] Chavanne, J., *et al. In-Vacuum Undulators at ESRF.* In *The 2003 Particle Accelerator Conference*, pages 253–255. Portland, Oregon USA (2003).

[3] Hara, T., *et al. In-vacuum undulators of SPring-8.* Journal of Synchrotron Radiation, **5**, pages 403–405 (1998).

[4] Rakowsky, G., *et al. NSLS in-vacuum undulators and mini-beta straights.* In *The 2001 Particle Accelerator Conference (PAC 2001)*, pages 2453–2455. Chicago, Illinois,USA (2001).

[5] Hara, T., *et al. Cryogenic permanent magnet undulators.* Phys. Rev. ST Accel. Beams, **7** (5), page 050702 (May 2004). doi:10.1103/PhysRevSTAB.7.050702.

[6] Kitegi, C., *et al. Development of a Cryogenic Permanent Magnet In-Vacuum Undulator at the ESRF.* In *The tenth European Particle Accelerator Conference, EPAC'06*, pages 3559–3561. Edinburgh, Scotland (2006).

[7] Chavanne, J., *et al. First operational experience with a cryogenic permanent magnet undulator at the ESRF.* In *The 23rd Particle Accelerator Conference*, pages 2414–2416. Vancouver, British Columbia, Canada (2009).

[8] Chao, A. W. and M. Tigner. *Handbook of Accelerator Physics and Engineering (3rd printing)* (2006).

[9] Walker, R. *Interference effects in undulator and wiggler radiation sources.* Nucl. Instr. and Meth. A, **335** (1-2), pages 328 – 337 (1993). ISSN 0168-9002. doi:DOI:10.1016/0168-9002(93)90288-S.

[10] Temnykh, A. B. *Measurement of NdFeB permanent magnets demagnetization induced by high energy electron radiation.* Nucl. Instr. and Meth. A, **587** (1), pages 13 – 19 (2008). ISSN 0168-9002. doi:DOI:10.1016/j.nima.2008.01.002.

[11] Temnykh, A. B. *Delta undulator for Cornell energy recovery linac.* Phys. Rev. ST Accel. Beams, **11** (12), page 120702 (Dec 2008). doi:10.1103/PhysRevSTAB.11.120702.

[12] Carr, R. *Adjustable phase insertion devices as X-ray sources.* Nucl. Instr. and Meth. A, **306** (1-2), pages 391 – 396 (1991). ISSN 0168-9002. doi:DOI:10.1016/0168-9002(91)90346-R.

[13] Bahrdt, J., *et al. Undulators for the BESSY Soft-X-Ray FEL.* pages 610–613 (2004).

[14] Onuki, H. *Elliptically polarized synchrotron radiation source with crossed and retarded magnetic fields.* Nucl. Instr. and Meth. A, **246** (1-3), pages 94 – 98 (1986). ISSN 0168-9002. doi:DOI:10.1016/0168-9002(86)90053-7.

[15] Volby, P. *Helical Undulator For Producing Circularly Polarized Photons," Workshop on new kinds of positron sources for linear collider*. Published as slac-r-502, SLAC (1997). 1997 Proceedings of the Workshop on New Kinds of Positron Sources for Linear Colliders SLAC: http://www.slac.stanford.edu/cgi-wrap/getdoc/nkpslc97-015.pdf.

[16] Elleaume, P., J. Chavanne, and B. Faatz. *Design considerations for a 1 Å SASE undulator*. Nucl. Instr. and Meth. A, **455** (3), pages 503 – 523 (2000). ISSN 0168-9002. doi:DOI: 10.1016/S0168-9002(00)00544-1.

[17] Temnykh, A. *Evaluation of Magnetic and Mechanical Properties of Delta Undulator Model*. Technical Report CBN-09-01, , Cornell University, LEPP (2009). http://www.lns.cornell.edu/public/CBN/2009/CBN09-1/CBN_09-01.pdf.

[18] O'Hanlon, J. F. *A Users Guide to Vacuum Technology*. Second edition.

[19] Li, Y. *ADC In-Vacuum Undulator Magnet Material Out-gassing Test Report* (2008).

[20] Temnykh, A., *et al. Delta undulator model: Magnetic field and beam test results*. Nucl. Instr. and Meth. A, **In Press, Corrected Proof**, pages – (2010). ISSN 0168-9002. doi:DOI:10.1016/j.nima.2010.11.011.

[21] Anashin, V. V. *Superconducting Spiral Undulator for Measuring the Radiation Polarization Colliding Beams in the Vepp-2m Electron Positron Storage Ring*. Instruments and Experimental Techniques, **29 (6)**, pages 1267–1271 (1986).

[22] Mikhailichenko, A. *Wiggler for CESR operation at 2-GeV*. Technical Report CBN-04-07, Cornell University (May 2001).

[23] Rice, D., *et al. Production and testing considerations for CESR-c wiggler magnets*. In *the 2003 Particle Accelerator Conference*, volume 1, pages 167–169. Portland, OR (2003).

[24] Mikhailichenko, A. *Test of Short Period SC Undulator*. In *The eleventh European Particle Accelerator Conference, EPAC'08*, pages 595–597. Genoa, Italy (2008).

[25] Clarke, J., *et al. Construction of a full scale superconducting undulator module for the international linear collider position sources*. In *The eleventh European Particle Accelerator Conference, EPAC'08*, pages 709–711. Genoa, Italy (2008).

[26] Mikhailichenko, A. *SC Undulator and SC wiggler for the Cornell ERL*. In *16th Pan-American Synchrotron Radiation Instrumentation Conference*. Argonne National Laboratory, USA (2010).

[27] Alferov, D. F., Y. A. Bashmakov, and E. G. Bessonov. *Device for Obtaining Polarized Electromagnetic Radiation*. Zhurnal Tekhnicheskoi Fiziki. Authors Certificate No 538508, USSR.

[28] MERMAID- MEsh Routine for MAgnet Interactive Design. Sim Limited, 630058, Novosibirsk, P.O. Box 160, Russia.